NeuroImage 260 (2022) 119459

Contents lists available at ScienceDirect

NeuroImage

journal homepage: www.elsevier.com/locate/neuroimage

Reduced functional connectivity supports statistical learning of temporally distributed regularities

Jungtak Park[a,b,1], Karolina Janacsek[c,d,1], Dezso Nemeth[d,e,f], Hyeon-Ae Jeon[a,b,g,h,*]

[a] Department of Brain Sciences, Daegu Gyeongbuk Institute of Science and Technology (DGIST), Daegu 42988, Republic of Korea
[b] Institute of Brain Sciences, Daegu Gyeongbuk Institute of Science and Technology (DGIST), Daegu 42988, Republic of Korea
[c] Centre for Thinking and Learning, Institute for Lifecourse Development, School of Human Sciences, Faculty of Education, Health and Human Sciences, University of Greenwich, Old Royal Naval College, London SE10 9LS UK
[d] Institute of Psychology, ELTE Eötvös Loránd University, 1064 Budapest, Hungary
[e] Brain, Memory and Language Research Group, Institute of Cognitive Neuroscience and Psychology, Research Centre for Natural Sciences, 1117 Budapest, Hungary
[f] Lyon Neuroscience Research Center (CRNL), INSERM, CNRS, Université Claude Bernard Lyon 1, 69675 Bron, France
[g] Convergence Research Advance Center for Olfaction, Daegu Gyeongbuk Institute of Science and Technology (DGIST), Daegu, Korea.
[h] Partner Group of the Max Planck Institute for Human Cognitive and Brain Sciences at the Department of Brain and Cognitive Sciences, DGIST, Daegu 42988, Republic of Korea

ARTICLE INFO

Keywords:
Statistical learning
fMRI
Functional connectivity
Group ICA
ASRT

ABSTRACT

Statistical learning is a powerful ability that extracts regularities from our environment and makes predictions about future events. Using functional magnetic resonance imaging, we aimed to probe how a wide range of brain areas are intertwined to support statistical learning, characterising its architecture in the whole-brain functional connectivity (FC). Participants performed a statistical learning task of temporally distributed regularities. We used refined behavioural learning scores to associate individuals' learning performances with the FC changed by statistical learning. As a result, the learning performance was mediated by the activation strength in the lateral occipital cortex, angular gyrus, precuneus, anterior cingulate cortex, and superior frontal gyrus. Through a group independent component analysis, activations of the superior frontal network showed the largest correlation with the statistical learning performances. Seed-to-voxel whole-brain and seed-to-ROI FC analyses revealed that the FC between the superior frontal gyrus and the salience, language, and dorsal attention networks were reduced during statistical learning. We suggest that the weakened functional connections between the superior frontal gyrus and brain regions involved in top-down control processes serve a pivotal role in statistical learning, supporting better processing of novel information such as the extraction of new patterns from the environment.

1. Introduction

What would be the most fascinating and overarching ability in human behaviours? Grasping regularities from the world, learning them by degrees, and utilising them automatically in everyday life might be the answer. In our rapidly changing world, our brains continuously seek, attain, and cope with regularities. Scientists have named these processes 'statistical learning' (Armstrong et al., 2017; Aslin, 2017). Statistical learning is a powerful process that extracts regularities from our environment and makes predictions about future events. More surprisingly, one can perform statistical learning without awareness of the regularities or an explicit instruction, which is related to an unconscious and automatic attentional process (Fiser and Aslin, 2002; Perruchet and Pacton, 2006; Turk-Browne et al., 2005; Vékony et al., 2022). It has been known to support various cognitive processes such as perception (Orbán et al., 2008; Winkler et al., 2009; Yang and Purves, 2003), associative learning (Turk-Browne et al., 2010), predictive processing (Bar, 2007; Turk-Browne et al., 2010; Winkler et al., 2009), and the acquisition of automatic behaviours and skills including language (Hallgató et al., 2013; Kaufman et al., 2010; Ullman et al., 2020). Indeed, statistical learning is an essential process for adaptive human behaviours.

Functional connectivity is defined as statistical dependencies (e.g. correlation coefficients) among remote neurophysiological events of anatomically distinct brain regions (Friston, 2011). The statistical de-

* Corresponding author at 333 Techno Jungang-daero, Hyeonpung-eup, Dalseong-gun, Daegu, 42988, Republic of Korea
E-mail address: jeonha@dgist.ac.kr (H.-A. Jeon).
[1] These authors contributed equally to this work.

https://doi.org/10.1016/j.neuroimage.2022.119459.
Received 1 April 2022; Received in revised form 29 June 2022; Accepted 7 July 2022
Available online 9 July 2022.

pendency is used as vital information to classify subjects or to predict experimental factors (Friston, 1994; Shen, 2015). Numerous studies have highlighted the significance of functional connectivity, investigating the contributions of pathological conditions and behavioural traits to coherent patterns between brain regions (Bullmore and Sporns, 2009; Mohanty et al., 2020; Van Den Heuvel et al., 2009). To date, extensive research has been conducted on statistical learning that only focuses on the functional mapping of neural correlates involved in extracting and learning statistical regularities (Schapiro et al., 2017; Turk-Browne et al., 2010), instead of investigating how several regions are orchestrated together across the whole brain in relation to statistical learning. More specifically, functional magnetic resonance imaging (fMRI) studies on statistical learning have shown that the primary visual cortex and lateral occipital cortex are implicated in the early extraction of low-level visual information and category-specific visual information, respectively (Gheysen et al., 2011; Karlaftis et al., 2019; Karuza et al., 2017; Turk-Browne et al., 2010, 2009). Depending on the specific characteristics of experimental tasks, a different set of regions was reported to be actively involved in statistical learning: for example, the inferior parietal lobule, inferior frontal gyrus, and anterior cingulate for top-down modulation and the primary motor cortex, supplementary motor area, and primary somatosensory cortex for bottom-up sensory functions (Karlaftis et al., 2019; Karuza et al., 2017; Turk-Browne et al., 2010). However, few studies have investigated how functional connections across the whole brain support the acquisition of temporally distributed statistical regularities (Kahn et al., 2018; Karuza et al., 2017, 2016). Therefore, in the present study, we aimed to fill this gap by putting an emphasis on the functional connectivity through using fMRI data from healthy human participants, hoping to delineate how functional connectivity across the whole brain is modulated by statistical learning and how the neural trait of effective learning is manifested in large-scale functional connectivity.

The functional connectivity in statistical learning can offer the theoretical framework for explaining how distant brain regions are intertwined with statistical learning (Ambrus et al., 2020; Tóth et al., 2017). Earlier studies have shown distinct and separable brain networks for explicit and procedural learning (Yang and Li, 2012), and statistical learning depends on the procedural learning process (Fiser and Aslin, 2002; Perruchet and Pacton, 2006; Turk-Browne et al., 2005; Vékony et al., 2022). Therefore, functional connectivity patterns between statistical and explicit learning are expected to be different. Along with this, positive functional connectivity in the frontoparietal, visual, and motor areas was reported to mediate explicit learning (Sami and Miall, 2013; Sun et al., 2007). On the other hand, negative correlations were found between frontal functional connectivity and statistical learning performance (Tóth et al., 2017). In this study, Tóth and colleagues employed a predictable second-order transitional probability structure to define statistical learning scores, and they discovered a negative correlation between statistical learning scores and connectivity strength in the anterior brain regions in slow (theta) and fast (beta) oscillations, and the negative correlation increased as the learning progressed. In a different study (Ambrus et al., 2020), researchers used inhibitory transcranial magnetic stimulation to determine whether the frontal lobe and statistical learning are causally associated, and they found that disruption of the frontal lobe had a beneficial effect on statistical learning and consolidation processes. These previous results indicate a critical role of reduced frontal connectivity in statistical learning. However, the oscillatory functional connectivity is insufficient to identify which brain regions are critically interconnected during statistical learning.

In the present study, we aim at investigating this theoretical framework by focusing on the interconnected functional networks across the entire brain region. Thirty-five healthy young adults performed a statistical learning task in an MRI scanner. Participants were asked to respond to a series of visual stimuli as fast and accurately as they could (see Figure 1). Unbeknown to them, the location of subsequent stimuli followed a predictable second-order transitional probability structure (Howard and Howard, 1997; Kóbor et al., 2020). Statistical learning was evidenced by increasingly faster responses to the more predictable stimuli compared to the less predictable ones (Kobor et al., 2017; Park et al., 2020). We used a refined index of statistical learning (SL) as the difference in mean reaction times between predictable and less predictable trials to scrutinise whether participants successfully learned the statistical regularities. SL scores were used for further analyses as it controls for visual, motor and attentional requirements, general speedup due to practice, as well as the potential build-up of fatigue (Török et al., 2017). Using a whole-brain analysis with parametric modulation, we determined the brain regions in which neural activity was modulated by participants' statistical learning performance as quantified by the difference of mean reaction times between predictable and less predictable conditions. Additionally, a whole-brain seed-to-voxel and a separate seed-to-ROI functional connectivity were investigated to scrutinise how the discrete statistical learning-related regions interacted with the rest of the brain, along with the well-known large scale functional brain networks. We found that statistical learning was supported by reduced functional connections between multiple regions across the brain, particularly between the superior frontal gyrus and the salience, dorsal attention, and language networks. Finally, using a group independent component analysis (ICA), the superior frontal network emerged as a critical network for statistical learning.

2. Methods

2.1. Participants

Thirty-five healthy young adults of Korean nationality (mean age = 23.1 years, SD = 2.8; 17 females) participated in the study. All were right-handed with normal or corrected-to-normal vision. Every participant signed an informed consent form prior to the experiment. Four participants' data were excluded from the analysis due to low behavioural accuracy (i.e. below 80%) in the task. Therefore, the data of 31 participants (mean age = 23.0 years, SD = 2.8; 14 females) were used for the analysis. A sample size was computed using PASS software (https://www.ncss.com/software/pass/) based on a previous study (Park et al., 2020) that used the same statistical learning task. A minimum sample size of 19 was calculated to achieve 90% power to detect an effect size of 0.8 (Cohen's d) using a two-sided one-sample *t*-test with a significance level of 0.05, indicating that the sample size of 31 participants in the present study was enough to find a significant effect of statistical learning.

2.2. Task design and procedure

In the MRI scanner, participants performed an alternating serial reaction time (ASRT) task, which has been a commonly used method to elucidate statistical learning (Howard and Howard, 1997; Janacsek et al., 2015; Kobor et al., 2017; Song et al., 2008; Tóth et al., 2017). We separated the ASRT task into three runs, with a break of approximately one minute in between. Each run was composed of 12 task blocks (36 task blocks in total), with each block being alternated with a rest block (Figure 1A). A fixation cross was shown for 7.1 s in the rest block. Only the first run had five additional warm-up blocks at the beginning (85 warm-up trials for each block). The task block started with five warm-up trials followed by 80 target trials.

In each target trial, a stimulus (a dog's face) was presented for 500 ms in one of four positions (Figure 1B). Participants were asked to press a button corresponding to the target position as accurately and quickly as possible. A grey screen with four empty circles was shown between each trial (inter-trial interval: 120 ms). The warm-up trials were made up of a target stimulus being randomly presented in one of the four positions and were not included in the analysis. Every task block took 52.9 s and the entire ASRT task was composed of 41 blocks (5 warm-up and 36 task blocks), resulting in approximately 41 minutes for the entire

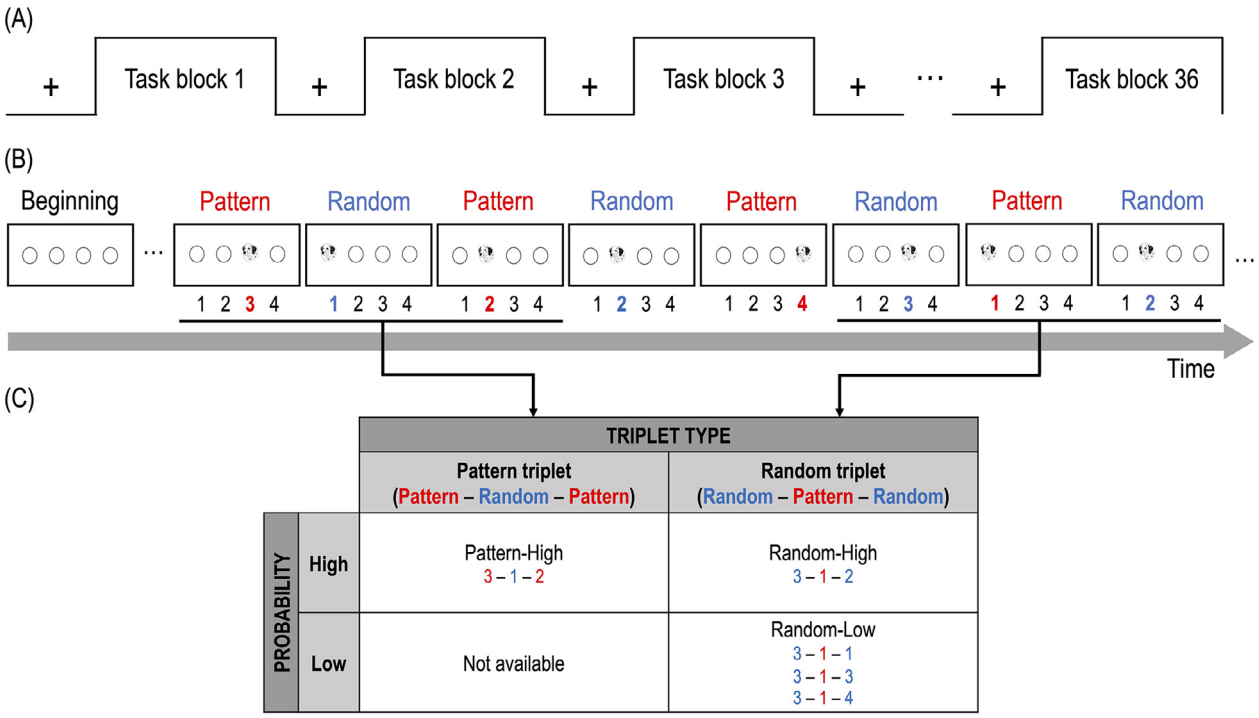

Fig. 1. Design of the ASRT task. (A) The ASRT task was composed of 36 task blocks with alternating rest blocks that are depicted as fixations in the figure. The task was divided into three scanning runs containing 12 task blocks for each. (B) A task block was composed of 5 warm-up trials and 80 target trials. Unbeknown to the participants, the target trials were composed of pattern and random trials that were presented alternately, constructing predictable and less predictable conditions. In each trial, a dog's face was shown for 500 ms as a target in one of the four circles, and participants were instructed to push the button corresponding to the target position. Four empty circles were presented between the target trials for 120 ms (not shown in this figure for ease of explanation). Here, the position of the target is indicated by the numbers in bold, which were not shown in the actual experiment. (C) For generating three conditions of Pattern-High, Random-High, and Random-Low, we combined three trials into a triplet. Probability indicates the number of occurrences (i.e., high probability or low probability). Triplet type is determined by a triplet composed of either Pattern-Random-Pattern (Pattern triplet) or Random-Pattern-Random (Random triplet). The example of Pattern-High ('3-1-2') denotes that the pattern trial ('2') is highly predictable after the pattern trial ('3') and random trial ('1'). Among the triplets in the random type, '3-1-2' is shown more frequently than others ('3-1-1', '3-1-3', '3-1-4'). Therefore, '3-1-2' is referred to as Random-High and others are Random-Low.

ASRT task. E-Prime 3.0 software (Schneider et al., 2002) was used for running the tests.

Unbeknown to the participants, there were two types of target trials—pattern type trials and random type trials (Figure 1B). Adopting these types, we constructed an alternating serial sequence made of four pattern trials being alternated with four random trials (i.e. eight trials in the sequence), and this sequence was repeated ten times in each block. This alternating serial sequence was individually determined in an order of permutation manner (e.g. 1r2r3r4r, 1r2r4r3r, …, 4r3r2r1r; r, random trials) to counterbalance the number of occurrences in every sequence. Within the sequence, the target stimulus was presented in a fixed position in the pattern trial and in a random position in the random trial. Any three consecutive target trials could establish a triplet (Howard and Howard, 1997; Howard et al., 2004) that occurred with high or low probability (Figure 1C). Please note that except for the first two subsequent target trials, all target trials were classified as the last item of a high or low probability triplet in a moving window manner. Notably, if a triplet had two pattern trials with one random trial (i.e. three consecutive trials of pattern-random-pattern), it was a pattern triplet with a high probability because the third pattern trial was predicted by the first pattern trial with a high probability. However, if a triplet had two random trials with one pattern trial (i.e. three consecutive trials of random-pattern-random), it was classified as a random triplet with either high or low probability, because some of the random triplets were identical to the pattern triplet with a high probability (i.e. Random-High, a random triplet with high probability). However, other triplets, which were not identical to the pattern triplet, had a low probability (i.e. Random-Low, a random triplet with low probability). The high probability triplets were presented five times more often than the low probability triplets (see Park et al., 2020 for further details). Here, comparing the high and low probability triplets in the same type (i.e. the random type triplet) enabled us to investigate the genuine effect of statistical learning because it depends only on the probability, controlling for other factors such as trial types or general speed (Park et al., 2020; Tóth et al., 2017). After the fMRI scanning, participants were asked if they noticed any regular patterns during the experiment. None of them reported regularities, suggesting participants were unaware of the structure of the alternating serial sequence.

2.3. MRI acquisition

Brain imaging data were collected using a 3T Siemens MAGNETOM Skyra Scanner (Siemens Healthcare, Erlangen, Germany) with a 64-channel phased-array head coil at Daegu-Gyeongbuk Medical Innovation Foundation (DGMIF). A high resolution T1-weighted structural image was collected (Tr = 2300 ms, TE = 3.44 ms, flip angle = 9°, FOV = 256 mm, and voxel size = 1 × 1 × 1 mm) at the beginning of the first scanning session with a magnetisation-prepared rapid gradient echo sequence (MPRAGE). Subsequently, a T2*-weighted gradient-echo echo-planar-imaging (EPI) sequence was used (Tr = 2000 ms, TE = 30 ms, flip angle = 90°, FOV = 192 mm, and in-plane resolution = 3 × 3 mm, and 30 slices of 4 mm thickness with a 20% gap) to acquire functional data covering the whole brain from the cerebellum to the vertex. The detailed information about raw fMRI data can be found in https://openneuro.org/datasets/ds003401/versions/1.0.1.

3. Data analysis

3.1. Behavioural analysis

We used only reaction times (RTs) of the correct trials in further analyses, since the participants' accuracy showed ceiling effects (overall accuracy: 91.4 %, SD = 0.7). Outliers were removed with a cut-off of two standard deviations from the mean RTs for each subject. To scrutinise whether or not participants successfully learned the statistical regularities, we defined statistical learning (SL) scores as the difference in mean reaction times (RTs) between the high probability triplets and low probability triplets of the same type (i.e., random type triplet). To calculate this score, we subtracted the mean RTs of the high probability triplets (Random-High) from those of the low probability triplets (Random-Low). Positive values represent the high performance of statistical learning (Armstrong et al., 2017; Aslin, 2017; Kobor et al., 2017; Reber, 1967; Tóth et al., 2017). The SL scores were tested against zero using a t-test to investigate the effects of statistical learning. Because an individual's overall RT could affect the individual SL scores, we used normalised RTs to calculate SL scores (Horváth et al., 2020; Zavecz et al., 2020). Normalisation was conducted as follows (1):

$$Normalised\ RT_{ij} = \frac{RT_{ij} - mean\ RT_i}{std(RT_i)};$$
$$\text{i : participant index; j : trial index} \quad (1)$$

SL scores were obtained from each block separately to investigate the behavioural changes as the statistical learning progressed over the learning time. Subsequently, a one-way analysis of variance (ANOVA) was used to examine whether or not there was a significant effect of the learning time (i.e. number of blocks) on participants' SL scores. We performed all the following analyses using Python 3 (Menczer et al., 2020) and MATLAB (Higham and Higham, 2016).

3.2. fMRI preprocessing

Preprocessing of fMRI data was done using the SPM12 software package (http://www.fil.ion.ucl.ac.uk/spm/) with the following steps: slice timing correction with the first slice as a reference slice, realignment to correct head motion artifacts using 6 affine head motion parameters, co-registration to individual T1 structural image, normalisation to Montreal Neurological Institute (MNI) template brain image, and smoothing with a Gaussian kernel of 6 mm full width at half maximum and resampling of functional images to 3 × 3 × 3 mm. Time series of BOLD signal were high-pass filtered to 1/128 Hz (128 s) to remove low-frequency components.

3.3. Whole-brain fMRI analysis

We analysed participants' brain activations using a generalised linear model (GLM). The brain data were concatenated across runs, and we added run regressors to eliminate run effect. The onsets of the task blocks were entered into the GLM as a task regressor with its duration of 52.9 s in a box-car function manner. We examined parametric modulation of neural activity by individual block-wise SL scores to scrutinise the activations that reflect the performance of statistical learning per block. To this end, we orthogonalised the task-related and SL-related effects by eliminating a collinearity between the task regressor and the parametric modulation regressor (i.e. SL scores) to investigate how the neural activity changes in association with the SL scores. Motion parameters from the realignment process were included in the GLM as regressors of no-interest to account for variance caused by head motion. An autoregressive AR(1) model with restricted maximum likelihood (ReML) estimation accounted for serial correlations due to unmodelled neuronal activity. The canonical hemodynamic response function (HRF) was convolved to model the hemodynamic response for every regressor. We calculated a one-tailed t-contrast for the SL-related parametric modulation regressor. Through these processes, we obtained individuals' contrast images of first-level analysis for the parametric modulation regressor-dependent BOLD signal, which were then entered into a group-level random-effects analysis. Results from the whole-brain analyses were thresholded at voxel level ($P < 0.001$ uncorrected), and only activations that survived at cluster level of false discovery rate (FDR) adjusted $P < 0.05$ were reported. A minimum cluster size with a cluster extent threshold of 24 was estimated using 3dClustSim (Forman et al., 1995), implemented in the AFNI software package (Cox, 1996; Cox and Hyde, 1997; Gold et al., 1998), and we reported clusters that have at least 24 significant voxels. For the assignment of MNI coordinates to the anatomical labelling, we used the Harvard-Oxford Cortical Structural Atlas (RRID:SCR_001476) (Kennedy et al., 1998; Makris et al., 1999) as distributed with FSL (FMRIB Software Library) (Jenkinson et al., 2012) unless specifically indicated. Brodmann areas were determined based on the peak coordinate of the clusters using MRIcron (Rorden and Brett, 2000) and Yale BioImage Suite Medical Image Analysis Software (Papademetris et al., 2006).

3.4. Whole-brain functional connectivity analysis using seed-to-voxel correlation

We explicitly selected seed regions that were found in the parametric modulation analysis and hypothesised that functional connectivity between the seed regions and other brain regions would be modulated by the SL task. To confirm this, the task-related functional connectivity in SL-related brain regions (obtained from the parametric modulation results) was tested using a whole-brain seed-to-voxel correlation analysis with CONN toolbox (www.nitrc.org/projects/conn, RRID:SCR_009550) (Whitfield-Gabrieli and Nieto-Castanon, 2012). First, we followed the CONN's default preprocessing pipeline: functional realignment and unwarp, slice-timing correction, outlier identification, direct segmentation and normalisation, and functional smoothing. The preprocessed data may still have contained non-neural signal or noise that originated from cerebral white matter, cerebrospinal areas, movement, outlier scans, or physiological sources. Since these residuals strongly influence functional connectivity, we additionally conducted two denoising steps, which were implemented within CONN's default denoising pipeline. As the first step, using linear regression, we removed potential confounding effects in the BOLD signal, such as noise components from white matter and cerebrospinal areas, realignment, scrubbing, and task effects (Behzadi et al., 2007; Friston et al., 1996; Power et al., 2014; Whitfield-Gabrieli and Nieto-Castanon, 2012). As the second step, temporal high-pass filtering was adopted to eliminate noise-related signals with low frequencies (threshold = 0.008 Hz). Then, using the denoised functional data, we explored individuals' task-related functional connectivity between the whole-brain voxels and predefined seed regions that were obtained from the parametric modulations of SL scores. To do this, we calculated participants' seed-based connectivity map by correlating the BOLD timeseries in each seed region and the BOLD timeseries in every voxel in the brain, using the Fisher-transformed bivariate correlation.

For the group-level analysis, participants' functional connectivity values (i.e. correlation coefficients) from the seed-based connectivity maps were concatenated and analysed with GLM to estimate the task-related functional connectivity (i.e. functional connectivity in the time window of task blocks) and rest-related functional connectivity (i.e. functional connectivity in the time window of rest blocks), using an ordinary least squares solution (Holmes and Friston, 1998). The two connectivity maps were compared to each other by F-contrast to find the task-induced changes in functional connectivity. For the functional connectivity results, we used thresholds of $P < 0.001$ uncorrected at voxel level and FDR adjusted $P < 0.05$ at the cluster level, with a cluster extent threshold of 24. Additionally, we averaged the correlation coefficients within the significant cluster (i.e. voxels) for each participant in the task

and rest time windows, separately. After that, we compared the mean correlation coefficients between the task and rest time windows (task > rest) using t-contrast to clarify whether the functional connectivity increased or decreased in the task.

3.5. Functional connectivity analysis using seed-to-ROI correlation

To further investigate SL-related regions with respect to certain cognitive functions, we calculated the functional connectivity between SL-related regions and the eight large-scale brain networks (provided by CONN toolbox) including default mode network (four ROIs), sensorimotor (three ROIs), visual (four ROIs), salience/cingulo-opercular (seven ROIs), dorsal attention (four ROIs), frontoparietal (four ROIs), language (four ROIs), and cerebellar (two ROIs) (Patil et al., 2021; Whitfield-Gabrieli and Nieto-Castanon, 2012). Since we aimed at investigating functional connectivity without bias, we used all these eight brain networks instead of selectively choosing specific brain networks/ROIs related to statistical learning. These networks were obtained from parcellation results of Human Connectome Project (HCP) dataset (497 subjects) using independent component analysis (ICA). They are considered to be the most common and consistently observed whole-brain resting-state networks (Yeo et al., 2011), characterizing several brain functions such as attention, memory, executive function, default mode, motor, and sensory systems (Biswal et al., 1995; Cole et al., 2010; Damoiseaux et al., 2006; De Luca et al., 2005; Dosenbach et al., 2007; Fox et al., 2006; Raichle et al., 2001; Vincent et al., 2008, 2006). Denoised functional data were used to calculate Fisher-transformed correlation coefficients between SL-related regions and the ROIs. In the group-level analysis, the correlation coefficients were contrasted (t-contrast) between the task and rest time windows (task > rest). In the seed-to-ROI correlation analysis, we used an uncorrected threshold $\alpha = 0.05$.

3.6. Data-driven functional connectivity with group independent component (ICA) analysis

To scrutinise the SL-related functional connectivity more thoroughly, we additionally took a data-driven approach, that is, group ICA. ICA decomposes data into the neural signals of interest and non interest, which helps to reveal the brain functions that cannot be explicitly modelled due to insufficient prior information (Hyvärinen and Oja, 2000). In the present study, group ICA was performed using GIFT toolbox (http://icatb.sourceforge.net/) (Calhoun et al., 2001). Prior to the ICA decomposition, data were temporally concatenated across participants, and data dimensions were reduced to 60 components using principle component analysis (PCA) since a relatively large number of principle components improve the performance of component reconstruction (Erhardt et al., 2011). After the PCA step, 40 independent components were extracted using the infomax algorithm, which uses a fixed nonlinearity for a higher-order Gaussian distribution (Bell and Sejnowski, 1995). The infomax algorithm is known to return stable and reliable results in most cases (Bell and Sejnowski, 1995). The 40 independent components were sorted by correlation coefficient between the time course of mean neural activity in the independent component and the time course of parametric modulation function that was estimated in the whole-brain fMRI analysis (i.e. the function that was calculated by convolving SL scores with HRF).

4. Results

4.1. Behavioural results

4.1.1. Reaction times and accuracies in the alternating serial reaction time (ASRT) task

Participants performed an ASRT task (Fig. 1) in which they were required to press a button corresponding to a target position. Overall, participants showed high accuracy (across three runs: 91.4 %, SD = 0.7; Run 1: 91.4 %, SD = 0.8; Run 2: 92.0 %, SD = 0.6; Run 3: 90.8 %, SD = 1.0) and fast reaction times (across three runs: 349.9 ms, SD = 3.8; Run 1: 356.6 ms, SD = 3.9; Run 2: 347.2 ms, SD = 3.8; Run 3: 346.1 ms, SD = 4.1), indicating that they successfully performed the ASRT task.

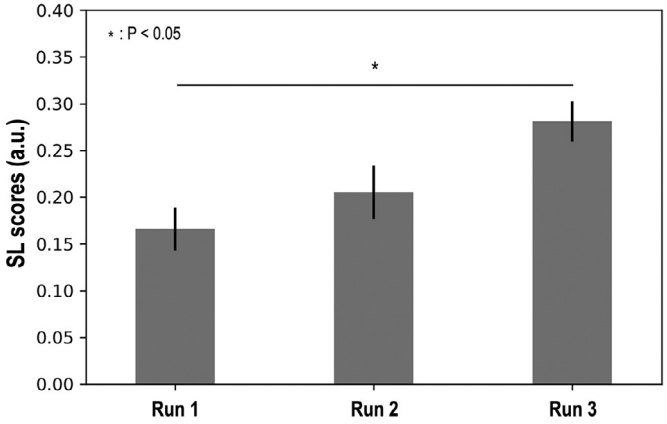

Fig. 2. SL scores in each scanning run. The x-axis and y-axis indicate the scanning run order and SL scores, respectively. Error bars indicate the standard error of the mean. Abbreviation: a.u., arbitrary unit.

4.1.2. Learning performance measured by statistical learning scores (SL scores)

We classified the stimuli into high and low probability and defined SL scores as differences of mean reaction times between them. Participants' SL scores were significantly higher than zero in the ASRT task [across three runs: $t(30) = 11.21$, $P = 3.0 \times 10^{-12}$; Run 1: $t(30) = 7.26$, $P = 4.4 \times 10^{-8}$; Run 2: $t(30) = 7.18$, $P = 5.4 \times 10^{-8}$; Run 3: $t(30) = 13.08$, $P = 6.2 \times 10^{-14}$] (Figure 2). These results indicate that participants successfully grasped probabilistic regularities in the ASRT task, and thus they responded faster to high probability triplets compared to the low probability ones. A one-way ANOVA with SL scores showed a significant main effect of the learning time (i.e. number of blocks) [$F(1,1114) = 19.65$, $P = 1.0 \times 10^{-5}$]. In the post-hoc analysis, we used the Bonferroni correction using a significance level of $\alpha = 0.05/3$ with a desired significance level $\alpha = 0.05$. SL scores were significantly higher in the third run compared to the first run [$t(30) = -3.666$, $P = 0.005$]. Specifically, participants achieved higher SL scores in the late phase of learning compared to the early phase of learning, indicating that they successfully grasped probabilistic regularities over the course of statistical learning.

4.2. Functional MRI results

4.2.1. Brain regions associated with statistical learning

Using parametric modulation analysis, we investigated which brain areas were significantly activated as participants improved their performances in statistical learning. We found five brain regions that were significantly modulated by SL scores: the right lateral occipital cortex, left angular gyrus, left precuneus, left anterior cingulate cortex, and left superior frontal gyrus (Fig. 3 and Table 1).

4.2.2. Whole-brain functional connectivity of the SL-related brain regions

We hypothesised that task-dependent functional connectivity would be observed in SL-related brain regions. To verify this, we first defined five seed regions that were obtained from the activations of parametric modulations by SL scores (see Figure 3 and Table 1). Second, we created seed-based connectivity maps derived from correlation coefficients between timeseries of the seed regions and the whole-brain voxels in the task and rest blocks, separately. Third, we explored task-related brain connectivity by comparing the task and rest seed-based connectivity maps (i.e. correlation coefficients) using F-contrast. Lastly, we compared the two connectivity maps using t-contrast to scrutinise the in-

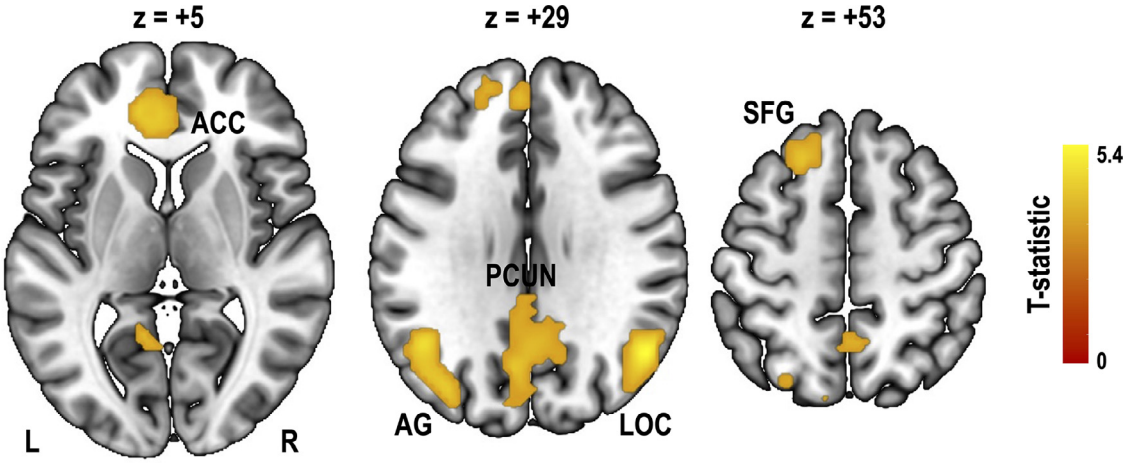

Fig. 3. SL-related brain activations. The brain regions associated with statistical learning were examined by the parametric modulation of task-related neural activity according to the SL scores. Abbreviations: L, left hemisphere; R, right hemisphere; ACC, anterior cingulate cortex; AG, angular gyrus; LOC, lateral occipital cortex; PCUN, precuneus; SFG, superior frontal gyrus.

Table 1
SL-related brain activations.

Brain regions	BA	Cluster size(voxels)	Z-value	MNI coordinates (mm)		
				x	y	z
R Lateral Occipital Cortex (superior division)	39	223	4.52	51	-61	29
L Angular Gyrus	39	419	4.08	-45	-58	29
L Precuneus	18	703	3.88	-6	-67	26
L Anterior Cingulate Cortex	32/11	344	3.84	-12	41	5
L Superior Frontal Gyrus	8	213	3.72	-18	26	53

Notes: Throughout the study, we used the Harvard-Oxford Cortical Structural Atlas (RRID:SCR_001476) (Kennedy et al., 1998; Makris et al., 1999) as distributed with FSL (FMRIB Software Library) (Jenkinson et al., 2012) for the assignment of MNI coordinates to the anatomical labelling, unless specifically indicated. Brodmann areas were determined based on the peak coordinate of the clusters using MRIcron (Rorden and Brett, 2000) and Yale BioImage Suite Medical Image Analysis Software (Papademetris et al., 2006). Abbreviations: BA, Brodmann area; L, left hemisphere; R, right hemisphere.

crease or decrease of connectivity during the task blocks in comparison with the rest blocks. As a result, we revealed significant connections between the seed regions and several brain clusters during statistical learning (Table 2, and Fig. 4 and Figure S1-4). Interestingly, most of these connections were weaker in the task blocks compared to the rest blocks (negative T-values in Table 2). In Fig. 4, we highlighted the result for the seed region of the left superior frontal gyrus because this area turned out to be specifically relevant for statistical learning in the analysis of data-driven group ICA (in the following Fig. 6). Results from the other four seed regions are displayed in Figure S1–4.

4.2.3. Functional connectivity between the SL-related brain regions and the large-scale intrinsic functional networks

To further investigate whether SL-related regions (Figure 3 and Table 1) are possibly associated with a number of intrinsic distributed networks whose topography indicates functional significance, we conducted seed-to-ROI correlation analysis focusing on the well-known large-scale intrinsic networks (i.e. the default mode, sensorimotor, visual, salience/cingulo-opercular, dorsal attention, frontoparietal, language, and cerebellar networks) (Patil et al., 2021; Whitfield-Gabrieli and Nieto-Castanon, 2012). These networks were composed of 32 ROIs (see Table S1 for the list of ROIs and CONN website for their locations [https://web.conn-toolbox.org/conn-in-pictures]). The seed regions were obtained from the SL-related brain regions (see Figure 3 and Table 1). A data-driven hierarchical clustering procedure (Sorensen, 1948) was used to display connectograms (Figure 5 and Figure S5-7) using Euclidean distances computed with connectivity strengths (i.e. functional criteria) and spatial locations (i.e. spatial criteria). All the connections between all pairs of ROIs were analysed using a multivariate parametric GLM analysis with an uncorrected threshold $\alpha = 0.05$ (Jafri et al., 2008). Consequently, the seed in the left superior frontal gyrus showed significantly decreased functional connectivity (i.e. correlation coefficients) with the salience, dorsal attention, and language networks in the task blocks compared to the rest blocks (Fig. 5).

The same analysis was performed on the other four SL-related regions (the right lateral occipital cortex, left angular gyrus, left precuneus, and left anterior cingulate cortex). The right lateral occipital cortex had one negative and one positive functional connection with the frontoparietal and default mode networks, respectively (Figure S5). The left angular gyrus showed negative functional connectivity with the four functional networks (i.e. the salience, dorsal attention, language, and visual networks) (Figure S6). Positive functional connectivity was observed between the left precuneus and default mode network (Figure S7). Lastly, no significant functional connections were observed between the anterior cingulate cortex and any of the intrinsic functional networks.

4.2.4. Data-driven SL-related functional network

We conducted a group independent component analysis (ICA) to address a data-driven functional network during statistical learning. By using ICA, we were able to reveal all the possible contributions of functional connectivity to statistical learning, not being biased by a priori information or hypothesis (Fox and Raichle, 2007). Among the 40 independent components identified by ICA, the BOLD timeseries in the 10th component (i.e. the superior frontal network; Fig. 6) showed the largest correlation coefficient with the time course of SL scores ($r = 0.164$), which was significantly higher than the coefficients of other components [$t(38) = -9.66$, $P = 8.8 \times 10^{-12}$]. This result suggests that the superior

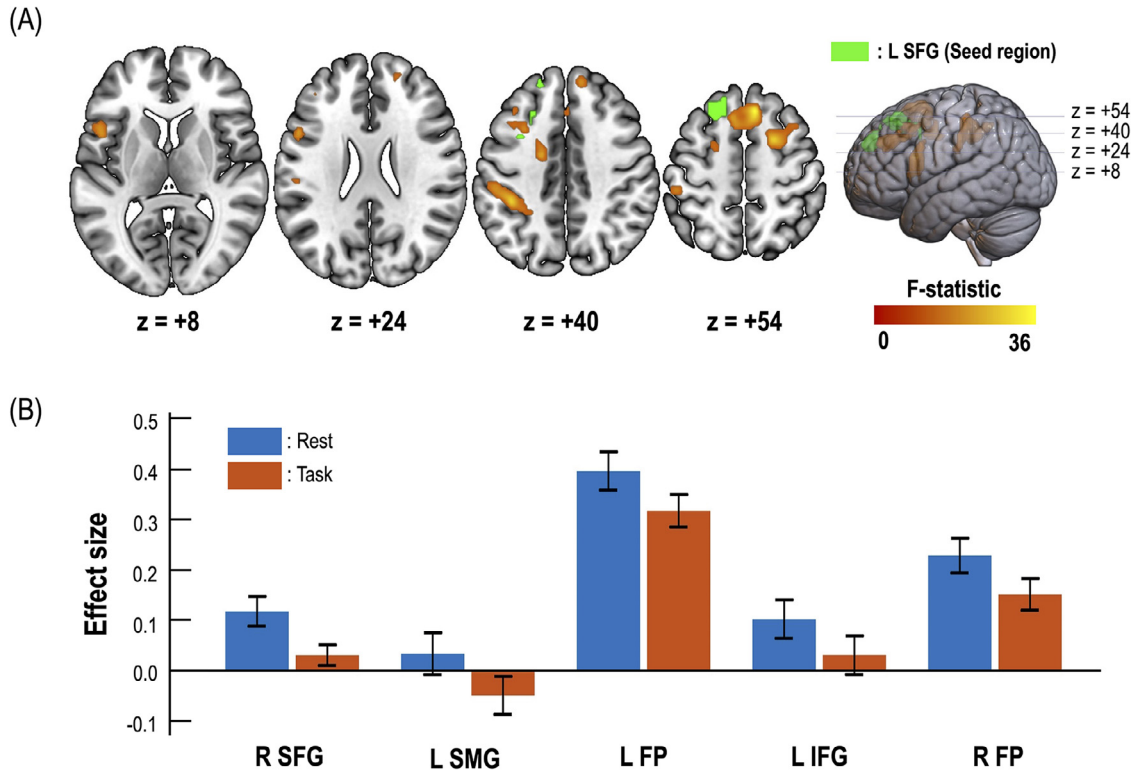

Fig. 4. Functional connectivity between the left superior frontal gyrus and voxels in the whole brain during the SL task. (A) The seed-to-voxel correlation was examined in the whole brain. The green colour represents the left superior gyrus as the seed region that is one of the SL-related brain regions. Results from the other four seed regions are displayed in Figure S1–4. (B) The effect sizes (i.e., correlation coefficients) indicate the strength of functional connectivity during the rest and task blocks. All functional connections shown here were weaker in the task blocks compared to the rest blocks, as indicated by the negative T-values in Table 2. Abbreviations: L, left; R, right; SFG, superior frontal gyrus; SMG, supramarginal gyrus; FP, frontal pole; IFG, inferior frontal gyrus.

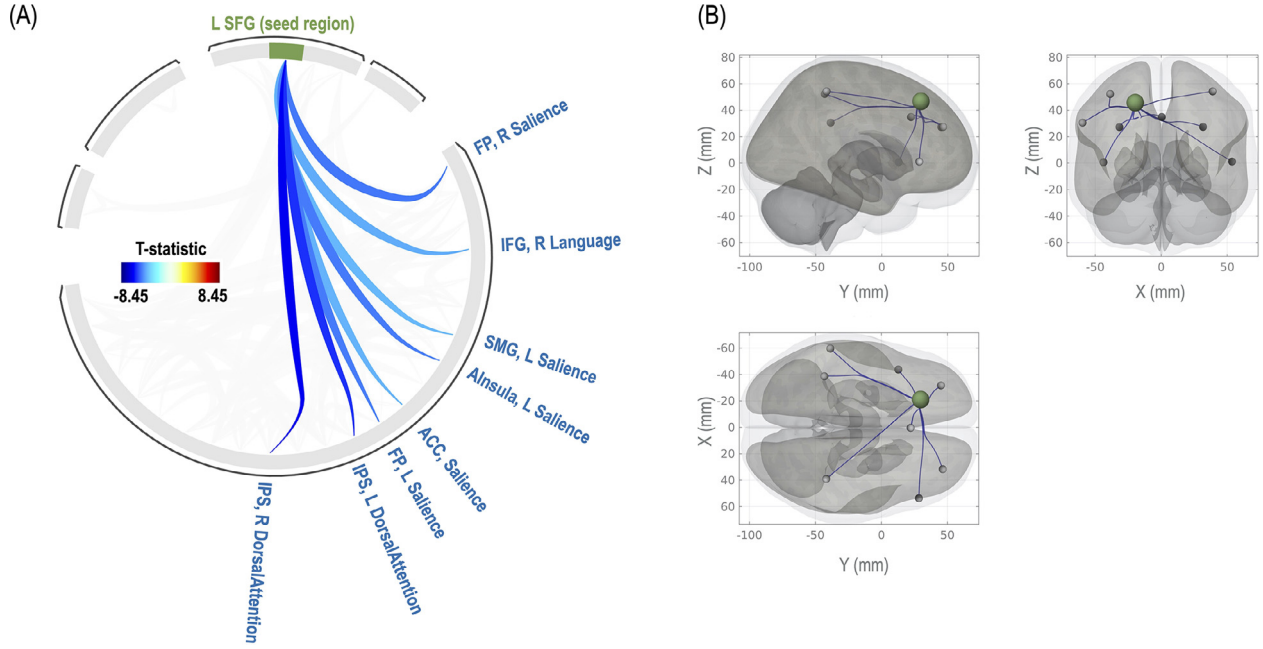

Fig. 5. Reduced functional connectivity between the left superior frontal gyrus and the salience, dorsal attention, and language networks during the SL task. (A) A connectogram indicated significantly decreased functional connectivity (uncorrected threshold $\alpha = 0.05$) between the left superior frontal gyrus (L SFG; the seed region) and eight ROIs located within the salience, dorsal attention, and language networks during the task blocks. (B) The eight functional connections were rendered in the 3D brain. The green and grey spheres denote the seed region (L SFG) and the eight ROIs, respectively. Here, only peak coordinates of the ROIs are shown for visualisation purposes. Connectograms with the other seed regions of the right lateral occipital cortex, left angular gyrus, and left precuneus are displayed in Figure S5-7. Abbreviations: L, left; R, right; SFG, superior frontal gyrus; FP, frontal pole; SMG, supramarginal gyrus; AInsula, anterior insular; ACC, anterior cingulate cortex; IPS, intraparietal sulcus.

Table 2
Task-related functional connectivity.

Seed regions	Brain areas	BA	Cluster size (voxels)	Z-value	T-value	MNI coordinates (mm)		
						x	y	z
R lateral Occipital Cortex	Cingulate Gyrus	-	242	4.37	-5.89	0	-14	26
L Angular Gyrus	L Angular Gyrus	40/39	1596	5.65	-10.21	-42	-52	38
	L Crus II‡	-	574	4.79	-7.62	-32	-64	-44
	L Inferior Frontal Gyrus	48/44	232	4.49	-6.30	-50	14	14
	L Cingulate Gyrus	-	213	4.44	-6.62	-4	-10	28
L Precuneus	R Superior Temporal Gyrus	21/38	437	5.59	6.53	52	2	-20
	L Superior Parietal Lobule	5/7	195	4.90	-5.87	-14	-52	60
	R WM Callosal body†	-	634	4.85	6.89	16	-48	24
	L Frontal Orbital Cortex	47	477	4.64	-6.84	-54	22	-8
	L WM Callosal body†	-	119	4.48	-6.53	-14	-10	34
	R Frontal Pole	46/10	248	4.32	-5.41	42	48	-2
	L WM Optic radiation†	-	241	4.31	-4.95	-14	-82	14
	R Superior Temporal Gyrus	21/22	383	4.22	-5.70	66	-22	2
L Anterior Cingulate Cortex	R Middle Frontal Gyrus	44/8	2608	6.11	-7.78	36	10	40
	R Middle Temporal Gyrus	21	703	5.63	-10.03	64	-36	-8
	R Superior Parietal Lobule	7/39	393	4.87	-5.59	32	-56	42
	R Vermis VI‡	-	355	4.43	5.17	6	-62	-24
	L Middle Frontal Gyrus	48/8	194	4.40	-5.29	-40	14	30
	R Superior Frontal Gyrus	8	473	4.40	-6.31	4	32	44
	L Lateral Occipital Cortex	19/7	277	4.28	-5.52	-22	-74	38
	L Postcentral Gyrus	4/1	573	4.23	5.91	-26	-30	62
	R Postcentral Gyrus	4	208	4.01	4.96	26	-28	64
L Superior Frontal Gyrus	R Superior Frontal Gyrus	8	1352	4.77	-6.86	8	26	54
	L Supramarginal Gyrus	40/1	638	4.41	-5.92	-38	-36	38
	L Inferior Frontal Gyrus, pars opercularis	44	292	4.40	-5.51	-50	12	20
	L Frontal Pole	46/9	397	4.24	-7.25	-32	38	32
	R Frontal Pole	9	150	4.07	-5.61	22	52	30

Notes: Z-values are calculated by converting F-statistics to Z scores, which indicate the functional connectivity strengths between seed regions and voxels of the cluster. The positive or negative T-values represent the higher or lower strength of functional connectivity in the task blocks compared to the rest blocks, respectively. Abbreviations: BA, Brodmann area; L, left hemisphere; R, right hemisphere; WM, white matter.

‡ Cerebellar Atlas (Schmahmann et al., 2000).

† Juelich Histological Atlas (Eickhoff et al., 2007).

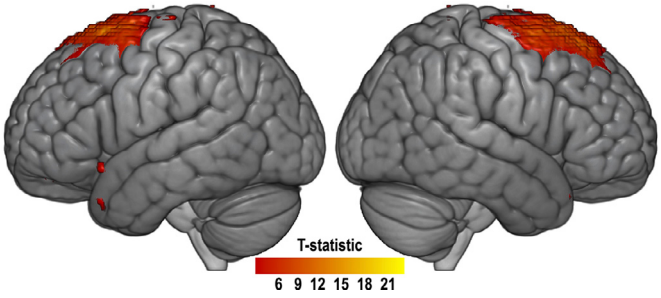

Fig. 6. Statistical learning dependent functional network. Group ICA revealed a network in the superior frontal area depicted by the red-yellow scale, showing a positive relationship with the SL scores.

frontal network constitutes a critical functional network for statistical learning.

From investigating the whole-brain functional connectivity (i.e. seed-to-voxel correlation) with the seed region of the left superior frontal gyrus (i.e. a SL-related region in the analysis of parametric modulation; Fig. 3 and Table 1), we found five task-related connections among which the strongest connectivity was observed between the left and right superior frontal gyri (the highest Z value [4.77] is shown in Table 2). These two areas showed decreased functional connectivity strength (i.e. correlation coefficient) in the task blocks compared to the rest blocks (Fig. 4B). This result, together with the group ICA result above, indicates that the superior frontal network and particularly the weakened functional connection between the left and right superior frontal gyri during task blocks compared to rest blocks is critical for statistical learning.

5. Discussion

The present study aimed to identify the brain regions and their functional connections underlying statistical learning of temporally distributed regularities. To this end, we used a statistical learning task with a well-controlled behavioural learning index (i.e. SL scores). Using a whole-brain parametric modulation analysis, we identified five discrete brain regions in which neural activity was associated with behavioural performances (i.e. SL scores). Next, we revealed how these regions interacted with the rest of the brain during statistical learning using functional connectivity analyses. Surprisingly, most of the SL-related areas had decreased functional connectivity across the voxels in the whole brain as participants progressed in statistical learning, and, specifically, the superior frontal gyrus had a strong and negative functional connectivity with the salience, dorsal attention, and language networks. Lastly, the group ICA underscored the critical role of the superior frontal network during the SL task. Thus, we provide a new framework to demonstrate the functional connectivity of statistical learning by various technical innovations and theoretical implications.

6. Multifaceted approaches for measuring functional connectivity

In the present study, we used three different methods to comprehensively elucidate the functional connectivity involved in statistical learning. First, using the seed-to-voxel correlation analysis in the whole brain with the seed regions associated with statistical learning (the lateral occipital cortex, angular gyrus, precuneus, anterior cingulate cortex, and superior frontal gyrus; see Figure 3 and Table 1), we revealed how spatially separated brain areas are functionally connected to each other with respect to statistical learning. Second, using a seed-to-ROI analysis we unveiled how SL-related regions are associated with the well-known large-scale functional networks (i.e. the default mode, sensorimotor, visual, salience/cingulo-opercular, dorsal attention, frontoparietal, language, and cerebellar networks). Finally, with the help of a group ICA we showed the most essential network intertwined with statistical learning. In particular, this data-driven approach enabled us to reveal the brain networks that may be hard to be explicitly modelled due to insufficient prior information (Hyvärinen and Oja, 2000). In other words, unlike traditional approaches, it is not required to determine predefined brain regions and condition-specific time series in ICA. Moreover, ICA can elicit meaningful components by denoising artifact-related independent components (Salman et al., 2019). In summary, by means of multifaceted approaches, we succeeded in rigorously elucidating the functional connections contributing to statistical learning.

7. Reduced functional connectivity beneficial to statistical learning

The superior frontal gyrus, as being covaried with behavioural scores in the parametric modulation (Figure 3) and having SL-related functional connections (Figure 5), needs further discussion. As outlined in the introduction, the present study's high and low probability triplets had the same amount of visual (i.e., spatial locations of stimuli) and motor (i.e., button responses) demands and differed only in their occurrence probability. This experimental manipulation is critical in generating stimulus regularity during statistical learning. A previous study also found greater activation in the SFG for objects of structured (predictable) triplets than for those of random (unpredictable) triplets (Otsuka and Saiki, 2020). In line with this, learning temporally distributed regularities in the present study seems to pertain to the involvement of the SFG. A more prevailing account of the association between the SFG and statistical learning can be provided in the functional connectivity results.

We should scrutinise the superior frontal gyrus in harmony with other brain regions comprising SL-related functional connections during statistical learning. When the brain works on acquiring novel information, it is more advantageous to rely on stimulus-driven bottom-up processes than complex goal-directed top-down processes (Ambrus et al., 2020; Tóth et al., 2017). More specifically, statistical learning is dependent more on bottom-up processes than on top-down processes, being constrained by lower level perceptual organisation (Emberson et al., 2013). This proposal was supported by previous findings, showing that statistical learning performance was negatively correlated with goal-directed control functions; better statistical learning was associated with weaker top-down control processes (Nemeth et al., 2013; Smalle et al., 2022; Virag et al., 2015). Likewise, a functional connectivity study using EEG phase synchronisation (Tóth et al., 2017) found a similar pattern, showing that statistical learning was negatively correlated with a large-scale functional neural network in slow (theta) and fast (beta) oscillations. Unfortunately, this study was not able to pinpoint the key nodes of this network because it did not use source localisation. However, thanks to the better spatial resolution of fMRI compared to EEG, we successfully provided more solid evidence of spatial locations for this antagonistic relationship by showing reduced functional connectivity in almost all connections, especially between the seed region of left superior frontal gyrus and the language, dorsal attention, and salience networks (Figure 5). More interestingly, these networks are involved in top-down processes such as goal-directed control, language, and attentional shifting functions, and thus their reduced connections with the left superior frontal gyrus may seem to implicate the dependency more on bottom-up processes than on top-down processes, leading to better statistical learning.

We should expound on why these three networks—the dorsal attention, salience, and language networks—were particularly mediated by statistical learning in the present study. The dorsal attention network and the salience network (also known as ventral attentional network) have been known to interplay with each other to mediate attentional control from top-down information and bottom-up sensory information (Uddin, 2015; Vossel et al., 2014). As mentioned above, attention is granted on statistical regularities aiding in effective statistical learning. Therefore, the link between the SL-related region (i.e. the superior frontal gyrus) and attention-related intrinsic functional networks (i.e. the dorsal attention and salience networks) can be construed as the integral role of attention in statistical learning.

Observation of the language network could be interpreted as a consequence of the complex relationship between statistical learning and language processing, not to mention attention. Important (but not exclusive) computations in language processing are grasping statistical relationships between inputs because language is composed of the statistical regularities among an infinite number of possible associations at various levels such as phonology, morphology, semantics, and syntax (Evans et al., 2009; Finn and Kam, 2008; Misyak et al., 2009). For example, one can learn a new word by extracting distributions of syllables, that is, how each syllable is likely to appear in connection with each other (Saffran et al., 1996). In the same vein, our participants were also actively involved in extracting statistical regularities from the incoming stimuli. Therefore, one of the critical characteristics of language processing and statistical learning—extracting regularities—seems to conjoin the SFG and the language network as one of the SL-related functional networks.

8. Limitation

In the present study, we used relatively short rest blocks (7.1 s) compared to task blocks (52.9 s). In general, block design fMRI experiments commonly use 10-30 s duration for rest blocks to obtain robust activation maps (Brockway, 2000; Elton and Gao, 2015; Jones et al., 2010; Jurkiewicz et al., 2018, 2007; Loubinoux et al., 2001; Mikulis et al., 2002). The relatively short duration of our rest blocks may have reduced the strength of task-related functional connectivity. Therefore, a future study is needed to use a lengthened duration for more robust results.

Another caveat to the present study is that a methodological limitation inherent to the fMRI, that is, observing hemodynamic responses correlated with neural activity (Constable, 2006), prevented us from examining a causal relationship between neural activations/functional connectivity and statistical learning in the present study. Therefore, it would be desirable to use non-invasive brain stimulation such as transcranial magnetic stimulation (TMS) to investigate the modulatory effects of the observed brain areas/connections on statistical learning in the future study.

9. Conclusion

Our findings in the present study offer detailed characterisation of the whole-brain functional brain architecture during statistical learning. We identified discrete brain regions and their interregional functional connectivity underlying the learning of temporally distributed statistical regularities through three functional connectivity analyses (i.e. seed-to-voxel whole-brain correlation analysis, seed-to-ROI correlation analysis, and group ICA). As a result, we unveiled the supporting role of the attenuated large-scale functional connectivity (e.g. between the left superior frontal gyrus and the salience, dorsal attention, and language networks)

in statistical learning. These findings may reflect a crucial mechanism of the brain, suggesting weaker functional connections with regions involved in goal-directed, top-down processes lead to better processing of novel information, including the extraction of new patterns from the environment.

Data and code availability statement

All raw MRI data was uploaded on 'OpenNeuro' (https://openneuro.org/datasets/ds003401/versions/1.0.1) and it is publicly available. The behavioral data and analysis code are released at https://github.com/jungtak05/Statistical-learning-fMRI-study.

Ethics statement

This study was approved by the Daegu Gyeongbuk Institute of Science and Technology (DGIST) ethics committee in accordance with the Declaration of Helsinki.

Declaration of Competing Interest

The authors report no competing interests.

Credit authorship contribution statement

Jungtak Park: Writing – original draft, Writing – review & editing, Methodology, Conceptualization, Formal analysis, Investigation, Visualization. **Karolina Janacsek:** Writing – original draft, Writing – review & editing, Methodology, Conceptualization. **Dezso Nemeth:** Writing – original draft, Writing – review & editing, Methodology, Conceptualization. **Hyeon-Ae Jeon:** Writing – original draft, Writing – review & editing, Conceptualization, Supervision, Project administration.

Acknowledgments

This research was supported by the Basic Science Research Program through the National Research Foundation of Korea (NRF) (NRF-2019M3C7A1031995, NRF-2020R1A2C2099568), and the Bio and Medical Technology Development Program of the NRF funded by MSIT (2017M3A9G8084463). This research was also supported by the National Brain Research Program (project 2017-1.2.1-NKP-2017-00002); Hungarian Scientific Research Fund (NKFIH-OTKA K 128016, to D.N., NKFIH-OTKA PD 124148 to K.J.); János Bolyai Research Scholarship of the Hungarian Academy of Sciences (to K.J.); IDEXLYON Fellowship of the University of Lyon as part of the Programme Investissements d'Avenir (ANR-16-IDEX-0005) (to D.N.). We thank Shameem Wagner and Romane Phelipon for their help in editing the manuscript.

Supplementary materials

Supplementary material associated with this article can be found, in the online version, at doi:10.1016/j.neuroimage.2022.119459.

References

Ambrus, GG, Vékony, T, Janacsek, K, Trimborn, ABC, Kovács, G, Nemeth, D., 2020. When less is more: Enhanced statistical learning of non-adjacent dependencies after disruption of bilateral DLPFC. J. Mem. Lang. 114, 104144. doi:10.1016/j.jml.2020.104144.

Armstrong, BC, Frost, R, Christiansen, MH., 2017. The long road of statistical learning research: past, present and future. Philos. Trans. R. Soc. Lond. B Biol. Sci. doi:10.1098/rstb.2016.0047.

Aslin, RN., 2017. Statistical learning: a powerful mechanism that operates by mere exposure. Wiley Interdiscip. Rev. Cogn. Sci. doi:10.1002/wcs.1373.

Bar, M., 2007. The proactive brain: using analogies and associations to generate predictions. Trends Cogn. Sci. 11, 280–289. doi:10.1016/j.tics.2007.05.005.

Behzadi, Y, Restom, K, Liau, J, Liu, TT., 2007. A component based noise correction method (CompCor) for BOLD and perfusion based fMRI. Neuroimage 37, 90–101.

Bell, AJ, Sejnowski, TJ., 1995. An Information-Maximization Approach to Blind Separation and Blind Deconvolution. Neural Comput. 7, 1129–1159. doi:10.1162/neco.1995.7.6.1129.

Biswal, B, Zerrin Yetkin, F, Haughton, VM, Hyde, JS., 1995. Functional connectivity in the motor cortex of resting human brain using echo-planar MRI. Magn. Reson. Med. 34, 537–541.

Brockway, JP., 2000. Two functional magnetic resonance imaging f (MRI) tasks that may replace the gold standard, Wada testing, for language lateralization while giving additional localization information. Brain Cogn. 43, 57–59.

Bullmore, E, Sporns, O., 2009. Complex brain networks: graph theoretical analysis of structural and functional systems. Nat. Rev. Neurosci. 10, 186–198.

Calhoun, VD, Adali, T, Pearlson, GD, Pekar, JJ., 2001. A method for making group inferences from functional MRI data using independent component analysis. Hum. Brain Mapp. 14, 140–151. doi:10.1002/hbm.1048.

Cole, MW, Pathak, S, Schneider, W., 2010. Identifying the brain's most globally connected regions. Neuroimage 49, 3132–3148.

Constable, RT., 2006. Challenges in fMRI and its limitationsFunctional MRI. Springer, pp. 75–98.

Cox, RW., 1996. AFNI: Software for Analysis and Visualization of Functional Magnetic Resonance Neuroimages. Comput. Biomed. Res. 29, 162–173. doi:10.1006/cbmr.1996.0014.

Cox, RW, Hyde, JS., 1997. Software tools for analysis and visualization of fMRI data. NMR Biomed. 10, 171–178. doi:10.1002/(SICI)1099-1492(199706/08)10:4/5<171::AID-NBM453>3.0.CO;2-L.

Damoiseaux, JS, Rombouts, S, Barkhof, F, Scheltens, P, Stam, CJ, Smith, SM, Beckmann, CF., 2006. Consistent resting-state networks across healthy subjects. Proc. Natl Acad. Sci. 103, 13848–13853.

De Luca, M, Smith, S, De Stefano, N, Federico, A, Matthews, PM., 2005. Blood oxygenation level dependent contrast resting state networks are relevant to functional activity in the neocortical sensorimotor system. Exp. Brain Res. 167, 587–594.

Dosenbach, NUF, Fair, DA, Miezin, FM, Cohen, AL, Wenger, KK, Dosenbach, RAT, Fox, MD, Snyder, AZ, Vincent, JL, Raichle, ME., 2007. Distinct brain networks for adaptive and stable task control in humans. Proc. Natl Acad. Sci. 104, 11073–11078.

Eickhoff, SB, Paus, T, Caspers, S, Grosbras, MH, Evans, AC, Zilles, K, Amunts, K., 2007. Assignment of functional activations to probabilistic cytoarchitectonic areas revisited. Neuroimage 36, 511–521. doi:10.1016/j.neuroimage.2007.03.060.

Elton, A, Gao, W., 2015. Task-positive functional connectivity of the default mode network transcends task domain. J. Cogn. Neurosci. 27, 2369–2381.

Emberson, LL, Liu, R, Zevin, JD., 2013. Is statistical learning constrained by lower level perceptual organization? Cognition 128, 82–102.

Erhardt, EB, Rachakonda, S, Bedrick, EJ, Allen, EA, Adali, T, Calhoun, VD., 2011. Comparison of multi-subject ICA methods for analysis of fMRI data. Hum. Brain Mapp. 32, 2075–2095. doi:10.1002/hbm.21170.

Evans, JL, Saffran, JR, Robe-Torres, K., 2009. Statistical learning in children with specific language impairment.

Finn, AS, Kam, CLH., 2008. The curse of knowledge: First language knowledge impairs adult learners' use of novel statistics for word segmentation. Cognition 108, 477–499.

Fiser, J, Aslin, RN., 2002. Statistical learning of higher-order temporal structure from visual shape sequences. J. Exp. Psychol. Learn. Mem. Cogn. 28, 458.

Forman, SD, Cohen, JD, Fitzgerald, M, Eddy, WF, Mintun, MA, Noll, DC., 1995. Improved Assessment of Significant Activation in Functional Magnetic Resonance Imaging (fMRI): Use of a Cluster-Size Threshold. Magn. Reson. Med. 33, 636–647. doi:10.1002/mrm.1910330508.

Fox, MD, Corbetta, M, Snyder, AZ, Vincent, JL, Raichle, ME., 2006. Spontaneous neuronal activity distinguishes human dorsal and ventral attention systems. Proc. Natl Acad. Sci. 103, 10046–10051.

Fox, MD, Raichle, ME., 2007. Spontaneous fluctuations in brain activity observed with functional magnetic resonance imaging. Nat. Rev. Neurosci. 8, 700–711.

Friston, KJ., 2011. Functional and effective connectivity: a review. Brain Connect. 1, 13–36.

Friston, KJ., 1994. Functional and effective connectivity in neuroimaging: a synthesis. Hum. Brain Mapp. 2, 56–78.

Friston, KJ, Williams, S, Howard, R, Frackowiak, RSJ, Turner, R., 1996. Movement-related effects in fMRI time-series. Magn. Reson. Med. 35, 346–355.

Gheysen, F, Van Opstal, F, Roggeman, C, Van Waelvelde, H, Fias, W., 2011. The Neural Basis of Implicit Perceptual Sequence Learning. Front. Hum. Neurosci. 5. doi:10.3389/fnhum.2011.00137.

Gold, S, Christian, B, Arndt, S, Zeien, G, Cizadlo, T, Johnson, DL, Flaum, M, Andreasen, NC., 1998. Functional MRI statistical software packages: A comparative analysis. Hum. Brain Mapp. 6, 73–84. doi:10.1002/(SICI)1097-0193(1998)6:2<73::AID-HBM1>3.0.CO;2-H.

Hallgató, E, Gyori-Dani, D, Pekár, J, Janacsek, K, Nemeth, D, 2013. The differential consolidation of perceptual and motor learning in skill acquisition. Cortex 49, 1073–1081. doi:10.1016/j.cortex.2012.01.002.

Higham, D., Higham, N., 2016. MATLAB guide, 150. SIAM, Philadelphia, PA.

Holmes, A, Friston, KJ., 1998. Generalisability, Random Effects & Population Inference. Neuroimage 7.

Horváth, K, Török, C, Pesthy, O, Nemeth, D, Janacsek, K., 2020. Divided attention does not affect the acquisition and consolidation of transitional probabilities. Sci. Rep. 10, 1–14. doi:10.1038/s41598-020-79232-y.

Howard, JH, Howard, D.V., 1997. Age differences in implicit learning of higher order dependencies in serial patterns. Psychol. Aging 12, 634–656. doi:10.1037/0882-7974.12.4.634.

Howard, D.V., Howard, JH, Japikse, K, DiYanni, C, Thompson, A, Somberg, R., 2004. Implicit sequence learning: effects of level of structure, adult age, and extended practice. Psychol. Aging 19, 79–92. doi:10.1037/0882-7974.19.1.79.

Hyvärinen, A, Oja, E., 2000. Independent component analysis: algorithms and applications. Neural Netw. 13, 411–430.

Jafri, MJ, Pearlson, GD, Stevens, M, Calhoun, VD., 2008. A method for functional network

connectivity among spatially independent resting-state components in schizophrenia. Neuroimage 39, 1666–1681.
Janacsek, K, Ambrus, GG, Paulus, W, Antal, A, Nemeth, D., 2015. Right hemisphere advantage in statistical learning: Evidence from a probabilistic sequence learning task. Brain Stimul. 8, 277–282. doi:10.1016/j.brs.2014.11.008.
Jenkinson, M, Beckmann, CF, Behrens, TEJ, Woolrich, MW, Smith, SM., 2012. Fsl. Neuroimage 62, 782–790. doi:10.1016/j.neuroimage.2011.09.015.
Jones, TB, Bandettini, PA, Kenworthy, L, Case, LK, Milleville, SC, Martin, A, Birn, RM, 2010. Sources of group differences in functional connectivity: an investigation applied to autism spectrum disorder. Neuroimage 49, 401–414.
Jurkiewicz, MT, Crawley, AP, Mikulis, DJ., 2018. Is rest really rest? Resting-state functional connectivity during rest and motor task paradigms. Brain Connect. 8, 268–275.
Jurkiewicz, MT, Mikulis, DJ, McIlroy, WE, Fehlings, MG, Verrier, MC., 2007. Sensorimotor cortical plasticity during recovery following spinal cord injury: a longitudinal fMRI study. Neurorehabil. Neural Repair 21, 527–538.
Kahn, AE, Karuza, EA, Vettel, JM, Bassett, DS., 2018. Network constraints on learnability of probabilistic motor sequences. Nat. Hum. Behav. 2, 936–947.
Karlaftis, VM, Giorgio, J, Vértes, PE, Wang, R, Shen, Y, Tino, P, Welchman, AE, Kourtzi, Z., 2019. Multimodal imaging of brain connectivity reveals predictors of individual decision strategy in statistical learning. Nat. Hum. Behav. 3, 297–307. doi:10.1038/s41562-018-0503-4.
Karuza, EA, Emberson, LL, Roser, ME, Cole, D, Aslin, RN, Fiser, J., 2017. Neural Signatures of Spatial Statistical Learning: Characterizing the Extraction of Structure from Complex Visual Scenes. J. Cogn. Neurosci. 29, 1963–1976. doi:10.1162/jocn_a_01182.
Karuza, EA, Thompson-Schill, SL, Bassett, DS., 2016. Local patterns to global architectures: influences of network topology on human learning. Trends Cogn. Sci. 20, 629–640.
Kaufman, SB, DeYoung, CG, Gray, JR, Jiménez, L, Brown, J, Mackintosh, N., 2010. Implicit learning as an ability. Cognition 116, 321–340. doi:10.1016/j.cognition.2010.05.011.
Kennedy, DN, Lange, N, Makris, N, Bates, J, Meyer, J, Caviness, VS, 1998. Gyri of the human neocortex: an MRI-based analysis of volume and variance. Cereb. Cortex 8, 372–384. doi:10.1093/cercor/8.4.372.
Kóbor, A, Horváth, K, Kardos, Z, Nemeth, D, Janacsek, K., 2020. Perceiving structure in unstructured stimuli: implicitly acquired prior knowledge impacts the processing of unpredictable transitional probabilities. Cognition 205, 104413.
Kobor, A, Janacsek, K, Takacs, A, Nemeth, D., 2017. Statistical learning leads to persistent memory: evidence for one-year consolidation. Sci. Rep. 7, 1–10. doi:10.1038/s41598-017-00807-3.
Loubinoux, I, Carel, C, Alary, F, Boulanouar, K, Viallard, G, Manelfe, C, Rascol, O, Celsis, P, Chollet, F., 2001. Within-session and between-session reproducibility of cerebral sensorimotor activation: a test–retest effect evidenced with functional magnetic resonance imaging. J. Cereb. Blood Flow Metab. 21, 592–607.
Makris, N, Meyer, JW, Bates, JF, Yeterian, EH, Kennedy, DN, Caviness, VS, 1999. MRI-based topographic parcellation of human cerebral white matter and nuclei. Neuroimage 9, 18–45. doi:10.1006/nimg.1998.0384.
Menczer, F, Fortunato, S, Davis, CA., 2020. Python tutorial. A First Course Netw. Sci. 221–237. doi:10.1017/9781108653947.010.
Mikulis, DJ, Jurkiewicz, MT, McIlroy, WE, Staines, WR, Rickards, L, Kalsi–Ryan, S, Crawley, AP, Fehlings, MG, Verrier, MC, 2002. Adaptation in the motor cortex following cervical spinal cord injury. Neurology 58, 794–801.
Misyak, JB, Christiansen, MH, Tomblin, JB., 2009. Statistical learning of nonadjacencies predicts on-line processing of long-distance dependencies in natural language. In: Proceedings of the Cognitive Science Society, pp. 177–182.
Mohanty, R, Sethares, WA, Nair, VA, Prabhakaran, V., 2020. Rethinking measures of functional connectivity via feature extraction. Sci. Rep. 10, 1–17.
Nemeth, D, Janacsek, K, Polner, B, Kovacs, ZA., 2013. Boosting human learning by hypnosis. Cereb. Cortex 23, 801–805. doi:10.1093/cercor/bhs068.
Orbán, G, Fiser, J, Aslin, RN, Lengyel, M., 2008. Bayesian learning of visual chunks by human observers. Proc. Natl Acad. Sci. 105, 2745–2750.
Otsuka, S, Saiki, J., 2020. Neural mechanisms of memory enhancement and impairment induced by visual statistical learning. J. Cogn. Neurosci. 32, 1749–1763.
Papademetris, X, Jackowski, MP, Rajeevan, N, DiStasio, M, Okuda, H, Constable, RT, Staib, LH., 2006. BioImage Suite: an integrated medical image analysis suite: An update. Insight J. 2006, 209.
Park, J, Yoon, HD, Yoo, T, Shin, M, Jeon, HA, 2020. Potential and efficiency of statistical learning closely intertwined with individuals' executive functions: a mathematical modeling study. Sci. Rep. 10. doi:10.1038/s41598-020-75157-8.
Patil, AU, Ghate, S, Madathil, D, Tzeng, OJL, Huang, H-W, Huang, C-M., 2021. Static and dynamic functional connectivity supports the configuration of brain networks associated with creative cognition. Sci. Rep. 11, 1–17.
Perruchet, P, Pacton, S., 2006. Implicit learning and statistical learning: one phenomenon, two approaches. Trends Cogn. Sci. 10, 233–238. doi:10.1016/j.tics.2006.03.006.
Power, JD, Mitra, A, Laumann, TO, Snyder, AZ, Schlaggar, BL, Petersen, SE., 2014. Methods to detect, characterize, and remove motion artifact in resting state fMRI. Neuroimage 84, 320–341.
Raichle, ME, MacLeod, AM, Snyder, AZ, Powers, WJ, Gusnard, DA, Shulman, GL., 2001. A default mode of brain function. Proc. Natl Acad. Sci. 98, 676–682.
Reber, AS., 1967. Implicit learning of artificial grammars. J. Verbal Learn. Verbal Behav. 6, 855–863. doi:10.1016/S0022-5371(67)80149-X.
Rorden, C, Brett, M., 2000. Stereotaxic display of brain lesions. Behav. Neurol. 12, 191–200.
Saffran, JR, Aslin, RN, Newport, EL., 1996. Statistical learning by 8-month-old infants. Science 274, 1926–1928 80.
Salman, MS, Du, Y, Lin, D, Fu, Z, Fedorov, A, Damaraju, E, Sui, J, Chen, J, Mayer, AR, Posse, S., 2019. Group ICA for identifying biomarkers in schizophrenia:'Adaptive'networks via spatially constrained ICA show more sensitivity to group differences than spatio-temporal regression. NeuroImage Clin. 22, 101747.
Sami, S, Miall, RC., 2013. Graph network analysis of immediate motor-learning induced changes in resting state BOLD. Front. Hum. Neurosci. 7, 166.
Schapiro, AC, Turk-Browne, NB, Botvinick, MM, Norman, KA, 2017. Complementary learning systems within the hippocampus: a neural network modelling approach to reconciling episodic memory with statistical learning. Philos Trans. R. Soc. B Biol. Sci. 372. doi:10.1098/rstb.2016.0049.
Schmahmann, JD, Doyon, J, Toga, AW, Petrides, M, Evans, AC., 2000. MRI Atlas of the Human Cerebellum. Acad Press.
Schneider, W, Eschman, A, Zuccolotto, A., 2002. E-Prime: User's Guide. Reference Guide. Getting Started Guide. Psychology Software Tools, Incorporated.
Shen, HH., 2015. Core concept: Resting-state connectivity. Proc. Natl Acad. Sci. 112, 14115–14116.
Smalle, EHM, Daikoku, T, Szmalec, A, Duyck, W, Möttönen, R., 2022. Unlocking adults' implicit statistical learning by cognitive depletion. Proc. Natl Acad. Sci. 119, e2026011119. doi:10.1073/pnas.2026011119.
Song, S, Howard, JH, Howard, D.V., 2008. Perceptual sequence learning in a serial reaction time task. Exp. Brain Res. 189, 145–158. doi:10.1007/s00221-008-1411-z.
Sorensen, TA., 1948. A method of establishing groups of equal amplitude in plant sociology based on similarity of species content and its application to analyses of the vegetation on Danish commons. Biol. Skar 5, 1–34.
Sun, FT, Miller, LM, Rao, AA, D'Esposito, M., 2007. Functional connectivity of cortical networks involved in bimanual motor sequence learning. Cereb. Cortex 17, 1227–1234.
Török, B, Janacsek, K, Nagy, DG, Orbán, G, Nemeth, D., 2017. Measuring and filtering reactive inhibition is essential for assessing serial decision making and learning. J. Exp. Psychol. Gen. 146, 529–542. doi:10.1037/xge0000288.
Tóth, B, Janacsek, K, Takács, Á, Kóbor, A, Zavecz, Z, Nemeth, D., 2017. Dynamics of EEG functional connectivity during statistical learning. Neurobiol. Learn. Mem. 144, 216–229. doi:10.1016/j.nlm.2017.07.015.
Turk-Browne, NB, Jungé, JA, Scholl, BJ, 2005. The automaticity of visual statistical learning. J. Exp. Psychol. Gen. 134, 552.
Turk-Browne, NB, Scholl, BJ, Chun, MM, Johnson, MK., 2009. Neural evidence of statistical learning: efficient detection of visual regularities without awareness. J. Cogn. Neurosci. 21, 1934–1945. doi:10.1162/jocn.2009.21131.
Turk-Browne, NB, Scholl, BJ, MK, Johnson, Chun, MM., 2010. Implicit perceptual anticipation triggered by statistical learning. J. Neurosci. 30, 11177–11187. doi:10.1523/JNEUROSCI.0858-10.2010.
Uddin, LQ., 2015. Salience processing and insular cortical function and dysfunction. Nat. Rev. Neurosci. 16, 55–61.
Ullman, MT, Earle, FS, Walenski, M, Janacsek, K., 2020. The neurocognition of developmental disorders of language. Annu. Rev. Psychol. doi:10.1146/annurev-psych-122216-011555.
Van Den Heuvel, MP, Mandl, RCW, Kahn, RS, Hulshoff Pol, HE, 2009. Functionally linked resting-state networks reflect the underlying structural connectivity architecture of the human brain. Hum. Brain Mapp. 30, 3127–3141.
Vékony, T, Ambrus, GG, Janacsek, K, Nemeth, D., 2022. Cautious or causal? Key implicit sequence learning paradigms should not be overlooked when assessing the role of DLPFC (Commentary on Prutean et al.). Cortex 148, 222–226.
Vincent, JL, Kahn, I, Snyder, AZ, Raichle, ME, Buckner, RL., 2008. Evidence for a frontoparietal control system revealed by intrinsic functional connectivity. J. Neurophysiol. 100, 3328–3342.
Vincent, JL, Snyder, AZ, Fox, MD, Shannon, BJ, Andrews, JR, Raichle, ME, Buckner, RL, 2006. Coherent spontaneous activity identifies a hippocampal-parietal memory network. J. Neurophysiol. 96, 3517–3531.
Virag, M, Janacsek, K, Horvath, A, Bujdoso, Z, Fabo, D, Nemeth, D, 2015. Competition between frontal lobe functions and implicit sequence learning: evidence from the long-term effects of alcohol. Exp. Brain Res. 233, 2081–2089. doi:10.1007/s00221-015-4279-8.
Vossel, S, Geng, JJ, Fink, GR., 2014. Dorsal and ventral attention systems: distinct neural circuits but collaborative roles. Neurosci 20, 150–159.
Whitfield-Gabrieli, S, Nieto-Castanon, A., 2012. Conn: a functional connectivity toolbox for correlated and anticorrelated brain networks. Brain Connect. 2, 125–141.
Winkler, I, Denham, SL, Nelken, I., 2009. Modeling the auditory scene: predictive regularity representations and perceptual objects. Trends Cogn. Sci. doi:10.1016/j.tics.2009.09.003.
Yang, J, Li, P., 2012. Brain networks of explicit and implicit learning. PLoS One 7. doi:10.1371/journal.pone.0042993.
Yang, Z, Purves, D, 2003. A statistical explanation of visual space. Nat. Neurosci. 6, 632–640.
Yeo, BTT, Krienen, FM, Sepulcre, J, Sabuncu, MR, Lashkari, D, Hollinshead, M, Roffman, JL, Smoller, JW, Zöllei, L, Polimeni, JR, 2011. The organization of the human cerebral cortex estimated by intrinsic functional connectivity. J. Neurophysiol..
Zavecz, Z, Horváth, K, Solymosi, P, Janacsek, K, Nemeth, D., 2020. Frontal-midline theta frequency and probabilistic learning: A transcranial alternating current stimulation study. Behav. Brain Res. 393. doi:10.1016/j.bbr.2020.112733.